Steric contribution of macromolecular crowding to the time and activation energy for preprotein translocation across the endoplasmic reticulum membrane

José Antonio Vélez Pérez[*] and Orlando Guzmán[†]
Departamento de Física, Universidad Autónoma Metropolitana–Iztapalapa, 09340 México, DF, México

Fernando Navarro-García[‡]
Department of Cell Biology, Cinvestav–Zacatenco, Ap. Postal 14-740, 07000 México, DF, México
(Received 19 December 2012; published 29 July 2013)

Protein translocation from the cytosol to the endoplasmic reticulum (ER) or vice versa, an essential process for cell function, includes the transport of preproteins destined to become secretory, luminal, or integral membrane proteins (translocation) or misfolded proteins returned to the cytoplasm to be degraded (retrotranslocation). An important aspect in this process that has not been fully studied is the molecular crowding at both sides of the ER membrane. By using models of polymers crossing a membrane through a pore, in an environment crowded by either static or dynamic spherical agents, we computed the following transport properties: the free energy, the activation energy, the force, and the transport times for translocation and retrotranslocation. Using experimental protein crowding data for the cytoplasm and ER sides, we showed that dynamic crowding, which resembles biological environments where proteins are translocated or retrotranslocated, increases markedly all the physical properties of translocation and retrotranslocation as compared with translocation in a diluted system. By contrast, transport properties in static crowded systems were similar to those in diluted conditions. In the dynamic regime, the effects of crowding were more notorious in the transport times, leading to a huge difference for large chains. We indicate that this difference is the result of the synergy between the free energy and the diffusivity of the translocating chain. That synergy leads to translocation rates similar to experimental measures in diluted systems, which indicates that the effects of crowding can be measured. Our data also indicate that effects of crowding cannot be neglected when studying translocation because protein dynamic crowding has a relevant steric contribution, which changes the properties of translocation.

DOI: 10.1103/PhysRevE.88.012725 PACS number(s): 87.15.−v, 47.63.mh, 87.16.−b, 36.20.−r

I. INTRODUCTION

Protein synthesis by ribosomes occurs in the cytoplasm. From there, preprotein chains destined to become secretory, luminal, or integral membrane proteins, transit to the ER lumen in a process known as translocation. On the other hand, retrotranslocation or dislocation refer to the transport of peptide chains in the opposite direction [1,2], as in the case of misfolded proteins that have to return to the cytoplasm to be degraded, or for some bacterial toxins associated with gastrointestinal diseases [3].

If translocation occurs while the peptide chain is being synthesized, it is dubbed as cotranslational; if it occurs after synthesis, it is called posttranslational. For cotranslational cases, the *in vivo* translocation speed is limited by the ribosome synthesis rate: in prokaryotes, it is 15–20 amino acids (aa) per second, and in eukaryotes is 3–4 aa/s [4]. For posttranslational translocation, *in vitro* experiments using inverted membrane vesicles and proteoliposomes yield translocation rates of 0.8–8 aa/s [5–7]. However, since these experiments have been performed only in a diluted regime, with soluble protein concentrations on the order of a few millimoles per liter, the effect of macromolecular crowding on protein translocation has not been measured.

Transport of biopolymers across membranes in cells, such as preproteins [8,9] and phage DNA [10], takes place between highly crowded media. The cytoplasm of a typical prokaryote (for instance, *Escherichia coli* K-12) has a protein concentration between 200 and 320 mg/ml [11]. By contrast, the protein concentration in the cytoplasm of eukaryotic cells is in the range 100–310 mg/ml [12–15]. In the lumen of the endoplasmic reticulum (ER), it is between 100–200 mg/ml [16–18].

Macromolecular crowding can have important effects on biological processes; it can increase the chemical activity of reactants by several orders of magnitude, reduce the diffusivity of proteins and nucleic acids, reduce renaturing yields, or even cause aggregation of proteins [19–21]. A preprotein transported between two media crowded by proteins should interact with these macromolecules, and chief among their nonspecific interactions is the steric hindrance due to excluded volume. Of course, in addition to concentration, several properties of the host media such as diffusivity, pH, among others would add to contrasting differences between the environments at either side of the membrane.

In this work, we investigated the effect of macromolecular crowding on protein translocation, using simple models for the translocation and retrotranslocation of proteins. We focused on the effect of having different concentration of proteins and diffusivities in the cytoplasm and ER lumen, and on significant differences between translocation under diluted and crowded conditions. For macromolecules, diffusivity in cellular environments can be several orders of magnitude

[*]josevel81@hotmail.com
[†]ogl@xanum.uam.mx
[‡]fnavarro@cell.cinvestav.mx

slower than in pure water; recent experiments have reported subdiffusion for biopolymers such as ribosomes, lipid granules, and chromosome loci [22–24]. Specifically, we applied a recent model proposed by Gopinathan and Kim for polymer translocation in crowded situations [25], and compared its mean first-passage time and activation energy needed to cross the membrane with the corresponding values in the diluted-conditions model of Sung and Park [26]. Both of these models consider normal diffusion only.

To this end, we considered in these models the number $n(t)$ of residues of the chain that have crossed the membrane as a stochastic variable, and then associated to it a free energy $F(n)$ due to the steric interaction of the chain with the crowding agents.

We found that the activation energy for translocation could be higher and grew faster with the chain size N in crowded environments than in diluted conditions. We also found that the translocation force remained of the same order than in diluted conditions but decayed more slowly with the number of translocated residues. Calculation of the mean first-passage time requires a model for the diffusion coefficient D of the preprotein as a function of n. We propose an extension of Sung and Park's interpolation formula for $D(n)$ to allow for different diffusivities at either side of the membrane, and dependence of said diffusivities with macromolecular crowding conditions. We parametrized this model for $D(n)$ using experimental data and found that the translocation time could be smaller than the retrotranslocation time, even when the concentration of proteins in the ER lumen was smaller than in the cytoplasm. The translocation time increased steeply with chain size: For chains of about 500 kDa, it became comparable with experimental data reported for diluted systems; however, for proteins of a few kDa, it was much smaller.

These results highlight the role of macromolecular crowding of the media (at both sides of a membrane) on the energies, forces, and times for translocation of preproteins of different size.

II. TRANSLOCATION MODELS FOR CROWDED AND DILUTED CONDITIONS

For translocation to occur, a peptide chain must interact in a complex and specific way with soluble and membrane proteins. For instance, the chain must include a signal sequence recognized by a specific receptor. They interact with the translocon channel and the chain enters the translocon pore, which permits transport between cytoplasm and ER. Among the many interactions involved in the process [27–29], we focused solely in the steric interactions with the membrane and soluble proteins at either side of it.

We studied models of translocation that take into account only steric interactions for an ideal chain of N monomers. The chain goes from the *cis* side to the *trans* side through a pore in a rigid, impermeable membrane (see Fig. 1). Specifically, we compared the results of a model for translocation of ideal chains between two identical and diluted milieus proposed by Sung and Park [26] [see Fig. 1(a)] with the results from two models proposed by Gopinathan and Kim for translocation between crowded environments [25] [Figs. 1(b) and 1(c)].

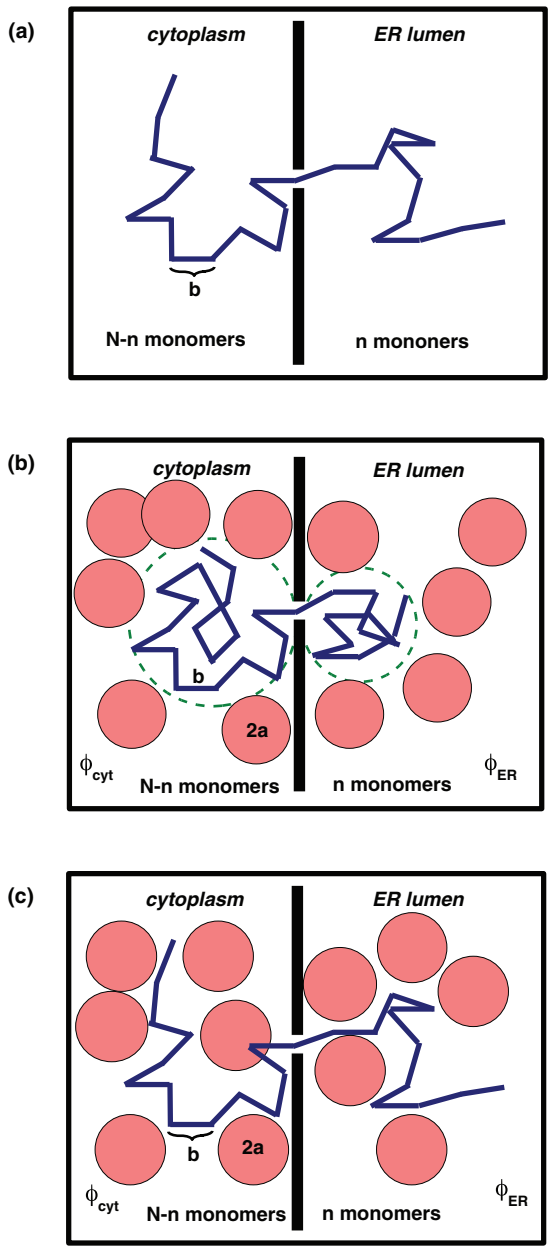

FIG. 1. (Color online) Schematic representation of three regimes for translocation of preprotein chains between cytoplasm and endoplasmic reticulum (ER) lumen: (a) diluted regime without obstacles, (b) dynamic-crowding regime with fast-moving obstacles, and (c) static-crowding regime with immobile obstacles. The translocating chain has N monomers of length b while the crowding agents have radius a. The volume fraction occupied by the crowding agents in the cytoplasm is $\phi_{\rm cyt}$ and in the ER lumen is $\phi_{\rm ER}$. At time t, the number of translocated monomers is n.

In crowded and diluted cases, the presence of the rigid wall modifies the free energy of the chain because it reduces the available conformations for the chain and thus modifies its entropy. In the crowded case, however, the models allow for spherical objects that exclude volume to each other and to the chain: This results in an additional contribution to the free energy of the system. Gopinathan and Kim identified two regimes amenable to theoretical characterization, based on the

dynamical behavior of the chain and crowding agents [25]. If the crowding agents move fast compared with the relaxation time of the polymer and the translocation time, one has a dynamic regime where it is possible to assume equilibrium statistics for polymer and crowding agents [see Fig. 1(b)]. Conversely, if the crowding agents move slowly compared with the translocation time (and the translocation time is still much larger than the relaxation time of the polymer), one has a static regime with equilibrium statistics for the polymer chain exploring a medium rich in immobile crowding agents [see Fig. 1(c)].

In all three cases, diluted regime and dynamic or static crowded regimes, the total free energy $\mathcal{F}(n)$ of the system can be expressed as a function of the number n of monomers at a given side of the membrane. Translocation can be modeled as a stochastic process described by a Fokker-Planck equation for the associated probability $P(n,t)$ of having n monomers at the *trans* side of the membrane at time t [25,26]:

$$\frac{\partial}{\partial t}P(n,t) = \left(\frac{1}{b^2}\left(\frac{\partial}{\partial n}\right)D(n)\exp\left[-\frac{\mathcal{F}(n)}{k_{\mathrm{B}}T}\right] \times \left(\frac{\partial}{\partial n}\right)\exp\left[\frac{\mathcal{F}(n)}{k_{\mathrm{B}}T}\right]\right)P(n,t), \quad (1)$$

where k_{B} is Boltzmann's constant, T is the temperature, b is the Kuhn length of the polymer, and the diffusivity of the chain is $D(n)$.

In this work, we characterized the translocation time τ as the mean first-passage time for the chain to go from a starting condition $n_0 = 1$ to a final situation with $n = N - 1$. Here, we did not take into account the time needed to insert the chain into the pore (going from $n = 0$ to $n = 1$) or release it after translocation (going from $n = N - 1$ to $n = N$). Thus, the translocation time is the average quantity $\tau(n,n_0) = \int_0^\infty t\omega(n_0,t)\,dt$, where $\omega = -\int_{n_0}^{N-1}\frac{\partial P}{\partial t}\,dn$ is the distribution of translocation times.

For the calculation of the translocation time, solving Eq. (1) for $P(n,t)$ can be omitted if one applies to that equation the Fokker-Planck operator adjunct to τ, thus obtaining a differential equation for τ itself [30]. This differential equation, when integrated, has the solution [31]

$$\tau = \int_1^{N-1} dn\,\frac{b^2}{D(n)}\exp\left(\frac{\mathcal{F}(n)}{k_{\mathrm{B}}T}\right)\int_1^n dm\,\exp\left(-\frac{\mathcal{F}(m)}{k_{\mathrm{B}}T}\right). \quad (2)$$

Equation (2) is the central relation that allows us to calculate the translocation time given the free energy $\mathcal{F}(n)$ and the diffusivity $D(n)$ in terms of the chain size N, the Kuhn length b, the crowding agent radius a, and volume fractions ϕ_{cyt} in the cytoplasm and ϕ_{ER} in the ER lumen.

Since explicit free energy models in terms of these parameters for the diluted system and crowded conditions are available from the works of Sung and Park [26] and Gopinathan and Kim [25], the main obstacle to obtain the translocation time was modeling the diffusivity of the chain $D(n)$. While Gopinathan and Kim assume a constant value $D(n) = D_P$, Sung and Park proposed an interpolation formula based on the diffusivity of the whole chain at the *cis* and *trans* sides of the membrane:

$$\frac{1}{D(n)} = \frac{n}{N}\frac{1}{D_{\mathrm{trans}}(N)} + \left(1 - \frac{n}{N}\right)\frac{1}{D_{\mathrm{cis}}(N)}. \quad (3)$$

In this work, we further generalized this equation to allow for variation of D_{cis} and D_{trans} with the volume fractions ϕ_{cyt} and ϕ_{ER}, in accordance with experimental data for the cytoplasm and the ER lumen.

A. Free energy models

Let $F(n,\phi)$ be the free energy for a chain segment of length n, with one end anchored to the pore, when it is immersed in a medium with volume fraction ϕ occupied by spherical crowding agents. Then, the total free energy of a chain with a total length N when n monomers are on the *trans* side of the membrane is

$$\mathcal{F}(n,\phi_{\mathrm{cis}},\phi_{\mathrm{trans}}) = F(N - n,\phi_{\mathrm{cis}}) + F(n,\phi_{\mathrm{trans}}). \quad (4)$$

For the diluted system, the free energy is proportional to the entropy reduction for a segment of length n anchored to the wall, relative to a free chain in the same environment [26]:

$$\frac{F_{\mathrm{dil}}(n)}{k_{\mathrm{B}}T} = \frac{1}{2}\log(n). \quad (5)$$

The physiologically relevant range for n and N can be determined by looking at the different lengths of proteins transported through the ER membrane. Small preproteins have masses on the order of 10 kDa and about 100 amino acids, such as prepromelittin (7.7 kDa, $N = 70$ aa [32,33]), or ERp18 (18 kDa, $N = 157$ aa [34,35]). Average-sized proteins have masses on the order of 50 kDa and several hundred amino acids; Ero1p is an example with a mass of 65 kDa and $N = 560$ aa [36,37]. Finally, there are a few large proteins with masses on the order of several hundred kDa and several thousand amino acids; ApoB is one example with mass $\approx$500 kDa and $N = 4536$ aa [38–41]. Considering these data, we set the following range:

$$n < N \leqslant N_{\max} = 4600. \quad (6)$$

In addition to the free energy due to chain-membrane interaction, there will be another contribution due to the excluded volume of the crowded agents. In the dynamic case, the free energy for a chain of n segments anchored at the wall is [25]

$$\frac{F_{\mathrm{dyn}}(n,\phi)}{k_{\mathrm{B}}T} = \frac{(1+\phi+\phi^2)\phi}{(1-\phi)^3}\left(\frac{n}{v}\right) - \frac{9(1+\phi)\phi^2}{2(1-\phi)^3}\left(\frac{n}{v}\right)^{2/3} + \frac{9\phi^3}{(1-\phi)^3}\left(\frac{n}{v}\right)^{1/3} + \frac{\pi^2}{6}n^{1/3}, \quad (7)$$

where $v = 4\pi(a/b)^3/3$ is the volume of a single crowding agent, in units of the Kuhn length of the chain. The first three terms represent the work against the crowding agents needed to create a cavity to confine the chain, as calculated by scaled particle theory [42], and the last term represents an entropy reduction due to confinement of the chain into the cavity [25,43].

As a first approximation, we took for the length b the distance between two consecutive amino acids in the amidic

plane, $b = 3.79$ Å; in an actual peptide chain the Kuhn length may be larger than this. Next, to define the size a of the crowding agents, we assumed that the main crowding agents in the cell are soluble proteins. For theoretical simplicity, we considered that the crowding agents at either side of the membrane are of the same species as the translocating chain; hence, all of them have the same length N. In practical terms, we set the radius of the crowding agents (at either *cis* or *trans* sides) as the radius of gyration of the translocated chains: $a = b(N/6)^{1/2}$.

For the crowding agents in the cytoplasm and ER lumen, we converted experimental ranges of protein concentration to volume fraction ranges, using the specific volume occupation reported by Zimmerman and Trach: 1.2 ml/g [44]. Protein concentrations have been found between 100 and 320 mg/ml in the cytoplasm [11–15], and between 100 and 200 mg/ml in the ER lumen [16]. Accordingly, the range for the volume fraction of crowding agents in the cytoplasm was

$$0.12 \leqslant \phi_{\text{cyt}} \leqslant 0.38, \tag{8}$$

and for the ER lumen the range was

$$0.12 \leqslant \phi_{\text{ER}} \leqslant 0.24. \tag{9}$$

These ranges agreed with experimental values of macromolecule occupation reported as relative dry mass concentration for the cytoplasm of different eukaryotic cells: kidney cells BHK-21, human glioma, Friend leukemia cells [45], and 3T3 fibroblasts [46]. The relative dry mass found on average was between 11% and 19% [45], but it was between 27% and 38% in regions of high protein concentration, composed primarily by protein fibers [45,46].

Now, for the static regime, the free energy contribution due to crowding can be obtained by thinking of the immobile obstacles as traps for a random walk that represents the ideal polymer chain [47–50]. The short- and long-chain limits of this static regime are defined by $n \ll N_C$ and $n \gg N_C$, respectively, where the crossover length, $N_C \sim (a/b)^2 \phi^{-3/2}$, has been estimated numerically as a function of ϕ by Barkema *et al*. [50]. Using this estimation and the ranges given for ϕ_{cyt} and ϕ_{ER}, we found that the short-chain limit is appropriate for all values n considered. Therefore, in the static limit the free energy of an n-monomer chain due to excluded volume by crowding agents is [25]

$$\frac{F_{\text{stat}}(n,\phi)}{k_{\text{B}}T} = \frac{1}{2}\left(\frac{b}{a}\right)^2 \phi\left(n + \sqrt{\frac{24a^2}{\pi b^2}n}\right). \tag{10}$$

B. Diffusivity models

We needed a generalization of Eq. (3) that allowed for dependence of diffusivity $D(n)$ with the volume fractions at either side of the wall. For this, we needed the functions $D_{\text{cis}} = D_{\text{cis}}(N,\phi_{\text{cis}})$ and $D_{\text{trans}} = D_{\text{trans}}(N,\phi_{\text{trans}})$. These are the diffusivities of chains residing entirely on the *cis* or *trans* sides; they depend both on the chain size N and the crowding-agent volume fraction ϕ in that side.

The diffusion of proteins and other macromolecules in crowded milieus can be measured using different crowding agents, such as other proteins and polymers [51,52]. The diffusion coefficient observed in these experiments can be factorized into two terms:

$$D(N,\phi) = D_0(N) f(\phi; a). \tag{11}$$

This type of factorization is commonly found for the diffusion coefficient of particles in gels [53], but from the work of Dauty and Verkman [51], as well as that of Banks and Fradin [52], it can be shown that the first term in Eq. (11) gives the dependence with chain size of the probe particle in pure solvent. For a polymer chain, $D_0(N)$ is expected to follow a power law: $D_0(N) = AN^{-p}$. This law corresponds to the model of Rouse if the exponent $p = 1$, and to the model of Zimm in Θ conditions if $p = 1/2$ [43]. The Rouse model ignores hydrodynamic interactions among monomers while the Zimm model does include them.

The second term in Eq. (11) accounts for the crowding agents' effect through its concentration and size: Experimental data can be fitted in a logarithmic fashion by the form [51,52],

$$\log f(\phi,a) = -B\phi^{\nu}, \tag{12}$$

with B and ν as adjustable parameters. The experiments show that ν may depend on the crowding-agent size: For Dextran of molecular weight between 1 and 400 kDa, ν varies between 0.8 and 1.4, with uncertainties on the order of 0.1 [52].

Therefore, based on the above results, we have assumed that the diffusion coefficient for chains entirely on either side of the membrane can be represented by the equation

$$\log D(N,\phi) = -p \log N + \log A - B\phi, \tag{13}$$

where p, A, and B were obtained from fits to experimental data for diffusion in the cytoplasm and ER lumen. As we explain below, the value $\nu = 1$ allowed us to fit the dependence with protein concentration accurately.

We were unable to find systematic measurements of protein diffusivities controlling simultaneously for chain size and crowding agent concentration; instead we found protein diffusivities as functions of either variable alone. For this reason, we had to determine coefficients p and B by fitting data independently with N and ϕ, and determine coefficient A by matching those independent fits to Eq. (13), as explained in detail in Appendix. We present next the results of that analysis for the cytoplasm and ER lumen.

First, we fitted data for diffusivities of proteins of different size in the cytoplasm of various cell types (see Table I). As illustrated in Fig. 2(a), we found that they could be fitted with $p = 1/2$ obtaining a determination coefficient $R^2 = 0.9720$. We also fitted data by Konopka *et al*. for the diffusivity of green fluorescent protein (GFP) in the cytoplasm of *Escherichia coli* [54]. Konopka and co-workers changed the protein concentration in the cytoplasm by growing cells under different values of osmolality (between 0.28 and 1.45 osm). Figure 2(b) shows that their data for cells adapted to such osmolality conditions are fitted with $B = 4.2 \pm 1.9$; the determination coefficient was $R^2 = 0.9725$. In brief, the model for the diffusivity for chains entirely in the cytoplasm turned out to be

$$D(N,\phi) = (433\ \mu\text{m}^2\,\text{s}^{-1})N^{-1/2}\exp(-4.2\phi). \tag{14}$$

For the ER, our search of the literature retrieved few data for protein diffusivities in the ER lumen as a function of protein size for a given cell type; Table II shows available data for

TABLE I. Protein diffusivities in the cytoplasm of different types of cells. All data were fitted to a power law $D(N) = AN^{-p}$ as shown in Fig. 2. The amino acid number was computed as the ratio between the molecular mass given in the references and the average molecular mass of amino acids (113 Da [59]), except for GFP whose number was taken from [60]. Diffusion coefficients of myoglobin from soleus cells with contractions and at 37 °C were not used in the fits; they are listed below to show a dependency of diffusivity on other factors.

Cell	Protein	N	$D(\mu\text{m}^2/\text{s})$
Muscle (20 °C) [55]	EGFP	239	15.8 ± 3
	Phosphoglucomutase	531	16.5 ± 3
	β-Enolase	796	10.8 ± 2
	IgG	1416	5.5 ± 1.0
Soma (20 °C) [56]	Lactalbumin	133	22.8 ± 1.7
	Ovalbumin	398	15.8 ± 2.1
	Bovine serum albumin	531	12.6 ± 1.5
Soleus (22 °C) [57]	Cytochrome c	110	13.0 ± 0.6
	Myoglobin	150	12.5 ± 1.3
	Hemoglobin	571	6.3 ± 0.5
	Catalase	2190	2.6 ± 0.4
Soleus with contractions (22 °C) [58]	Myoglobin	150	13.3 ± 0.7
Soleus (37 °C) [57]	Myoglobin	150	22.0 ± 1.2
Edl (22 °C) [57]	Cytochrome c	110	16.2 ± 0.6
	Myoglobin	150	18.7 ± 0.8
	Hemoglobin	571	6.2 ± 0.4
	Catalase	2190	1.9 ± 0.2

different cell types. A fit with $p = 1$ (Rouse model) accounts well for these data ($R^2 = 0.9098$), as illustrated in Fig. 2(a) as the solid red line. Next, we used experimental values of the diffusion coefficient in cells from Dayel *et al*. where the extracellular osmolalities were changed [16]. The measured value for the diffusion coefficient of GFP in the ER lumen of CHO-K1 cells was $7.5 \pm 2.5\ \mu\text{m}^2/\text{s}$. When the extracellular osmolality was changed, a 1.3-fold reduction of the diffusion coefficient occurred in going from 0.15-0.45 osm to 0.60 osm. Assuming that an increase in the external osmolality increases the protein content until it reaches its highest value at high osmolalities (that is, $\phi_{\text{ER}} = 0.24$), we estimated $B = 2.14 \pm 0.05$. In summary, the final model for the ER lumen diffusivity was

$$D_{\text{ER}}(N,\phi) = (2308\ \mu\text{m}^2\ \text{s}^{-1})N^{-1}\exp(-2.1\phi). \qquad (15)$$

Additionally to the crowded system, we need a model $D_{\text{dil}}(N)$ for particles diffusing in the diluted system: For the latter case, the milieus at both sides of the membrane are the same and Eq. (3) simplifies to $D(N,0) = D_{\text{dil}}(N)$. Arrio-Dupont *et al*. indicated that globular proteins of different size, at 20 °C, diffuse in water according to a power law $D \propto M^{1/3}$, with M being the molecular weight [55]. By taking M proportional to N, we fitted those diffusion coefficients using $D_{\text{dil}}(N) = AN^{-p}$ with $p = 1/3$ and we found $A = 509 \pm 27\ \mu\text{m}^2/\text{s}$. Diffusion coefficients for other globular proteins, measured at a similar temperature, 22 °C, reported by Sergey and Poo [56] and summarized by Papadopoulos [57], can be fitted with the same power law with a similar exponent ($p = 0.31 \pm 0.4$). Therefore, we used $D_{\text{dil}}(N) = 509\ \mu\text{m}^2\ \text{s}^{-1}N^{-1/3}$ in the calculations for the diluted system.

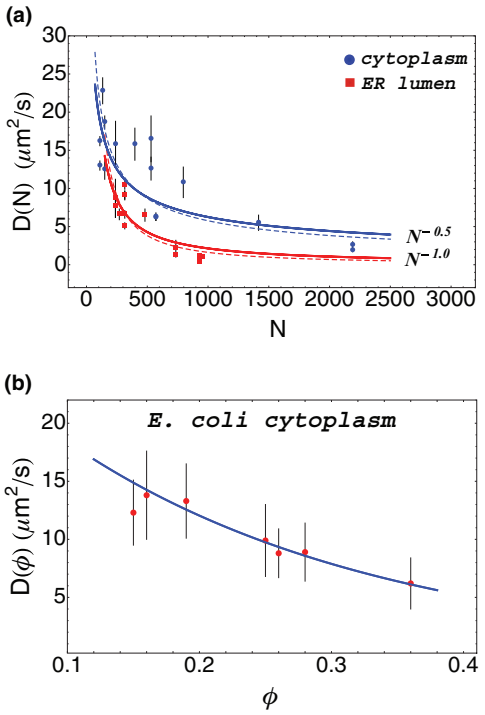

FIG. 2. (Color online) Fits to experimental data on the diffusion coefficients of proteins: (a) Diffusion coefficient as a function of chain size, $D(N)$, in the cytoplasm [55–58] and ER lumen [16,61–63], as detailed in Tables I and II. Dashed lines are fits to the power law $D(N) = AN^{-p}$ with A and p as adjustable parameters. The blue solid line is a fit to the Zimm model for cytoplasm (with $p = 1/2$); the red solid line is a fit to the Rouse model for the ER (with $p = 1$); in both cases, A was the sole adjustable parameter. (b) Diffusion coefficient of green fluorescent protein (GFP) as a function of volume fraction of cytoplasmic biopolymer [54]. The solid line is a fit to the exponential law $D(\phi) = B\exp(-\gamma\phi)$ with B and γ as adjustable parameters.

III. RESULTS

A. Validation of the dynamic-crowding regime conditions for translocation

Although it is clear that the crowding agents in the cytoplasm and ER lumen are mobile, we need to establish that protein translocation takes place in a dynamic regime. By substituting experimental values of diffusivity and viscosity for those milieus, we checked the conditions that define the static and dynamic regimes. Following Gopinathan and Kim, the two limiting regimes obey the conditions [25]:

$$\text{dynamic:} \quad \tau_o \ll \tau_r \ll \tau, \qquad (16)$$

$$\text{static:} \quad \tau_r \ll \tau \ll \tau_o, \qquad (17)$$

where τ_o is the time for obstacles motion, τ_r is the relaxation time of one chain, and τ is the translocation time. The first two are given by $\tau_o \sim C^{-2/3}/D_o$ and $\tau_r \sim (b^3/k_{\text{B}}T)\eta N^2$. In these expressions, C is the number density of obstacles, D_o is the diffusion coefficient of the crowding agents, and η is the viscosity of the milieu, which we consider parameters of

TABLE II. Protein diffusivities in the ER lumen of different types of cells. All data are reported at 37 °C except for GFP. We fitted them all to a power law $D(N) = AN^{-p}$ as shown in Fig. 2. The amino acid number was determined from the amino acid sequences of the fusion constructs, except for GFP whose number was taken from [60].

Cell	Protein	N	$D(\mu m^2/s)$
CHO-K1 [16]	GFP (23 °)	238	7.5 ± 2.5
K41-K42 [61]	ER-GFP	270	8.7 ± 2.5
	Crt-GFP	734	1.3 ± 0.3
	Crt-Y109F-GFP	734	2.2 ± 1.0
HepG2 [62]	ER-RFP	264	9.1 ± 0.6
	ER-GFP	270	6.6 ± 0.7
	BiP-GFP	932	0.60 ± 0.06
[63]	ER-RFP	264	6.5 ± 0.8
	BiP-GFP	932	1.08 ± 0.10
Cos7 [62]	ER-RFP	264	9.1 ± 0.5
	ER-RFP	264	10.4 ± 0.5
	BiP-GFP	932	1.1 ± 0.1
	BiP-GFP	932	1.2 ± 0.2
MDCK [62]	ER-RFP	264	5.1 ± 0.4
	BiP-GFP	932	0.32 ± 0.03
U2-OS [62]	ER-RFP	264	6.6 ± 0.5
	BiP-GFP	932	0.37 ± 0.03

the environment of interest. First, we discuss values for the cytoplasm, and then indicate what happens for the ER lumen.

In order to calculate the obstacle-motion time, τ_o, we computed the obstacle density in the cytoplasm as $C = cv_e/\frac{4}{3}\pi r^3$. In that expression, c is the protein concentration (between 100–320 mg/ml), v_e is the protein specific volume (1.2 ml/g) [44], and r is the radius of crowding agents, which we assumed as the radius of gyration R_g of translocating chains. For the diffusivity of crowders D_o, we used the cytoplasmic diffusion model given in Eq. (14). Then, for the least crowded condition in the cytoplasm (100 mg/ml or 0.12 in volume fraction), the time for obstacle motion scaled as $\tau_o \sim 979$ ps $N_o^{3/2}$, with N_o being the number of monomers of the crowding agents.

For the relaxation time τ_r, we needed the viscosity η. Data reported for the viscosity of the cytoplasm spans a wide range going from a few times the value for water [56,64–68] to a few hundred times that value [66,69].

We considered a value of 10 mPa·s for the viscosity and found that the relaxation time scaled as $\tau_r \sim 132$ ps N^2. Taking the size of crowding agents equal to that of translocating chains ($N_o = N$), we found that the leftmost dynamic-crowding condition in Eq. (16) is fulfilled for all known chains that translocate between the cytoplasm and the ER lumen; the rightmost condition was also satisfied when we considered the translocation times reported in Sec. III D. For even higher values of the viscosity, more than 100 times that of water for developing embryo cells [69], the separation between the relaxation time scale and the obstacle-motion time increases; therefore, the dynamic-crowding condition becomes a better approximation in such cases.

On the contrary, if we consider a small viscosity such as 2 mPa·s, just twice that of water, the relaxation time τ_r becomes much smaller than the obstacle-motion time τ_o for average size and smaller chains, being both similar for bigger chains like ApoB. Even when this small viscosity results in fulfillment of condition $\tau_r \ll \tau_o$, it does not give rise to a static regime: the translocation times computed for static crowded conditions in the next section turn out to be larger than the assumed obstacle-motion time τ_o; therefore, the static condition Eq. (17) is not satisfied. Instead, we expect that this type of crowding would lead to anomalous dynamics [25], which is beyond the scope of this work.

Finally, for the case of crowding in the ER lumen, its slower protein diffusion as compared with that in the cytoplasm, is indicative of a higher viscosity in such an environment, as stressed by Dayel *et al*. [16]. This situation corresponds to that of the cytoplasmic case at high viscosities discussed above; accordingly, the dynamic-crowding conditions in Eq. (16) would be satisfied more easily. Thus, the ER lumen behaves also as a dynamic-crowding environment.

B. Translocation free energy and activation energy are larger for dynamic-crowding than diluted systems

In order to compare translocation processes in the diluted and crowded systems, we analyzed the following variables: translocation free energy $\mathcal{F}$ and activation energy E_a, translocation force f, and mean first-passage time τ.

We started the analysis with the free energy of translocation $\mathcal{F}(n)$ since it will provide a basis for characterizing the activation energy E_a and the force $f(n)$ on the chain. It will also be needed for calculation of the mean transport time τ. We set $\mathcal{F}(N-1) = 0$, in order to measure the free energy relative to its value in a fully translocated chain, a convention that we used throughout this paper.

Using Eq. (4), we plotted in Fig. 3 the free energy as a function of the number of translocated monomers, for a chain of medium size (such as Ero1p, with $N = 560$) and compared the curve obtained for diluted conditions with the curves obtained for the dynamic- and static-crowding regimes. For the three cases, the free energy exhibited local minima when the chain was fully in the *cis* side or the *trans* side, and a single global maximum that acts as a barrier and introduces an activation energy for transport from one side to the other. We calculated two activation energies (E_a), one for translocation and another for retrotranslocation, as the difference between the free energy at the maximum and the minima for the *cis* side or the *trans* side, respectively.

For the diluted system, the maximum was attained when half of the chain had been translocated, and the two minimum values were equal. This is to be expected: The translocation and retrotranslocation processes in this case are equivalent because the media in both sides were the same. Therefore, the activation energies for translocation and retrotranslocation had the same value $E_a = 1.52$ kcal/mol.

For dynamic crowding, since the free energy given by Eq. (7) depends on concentrations, we analyzed the free energy curves in terms of the difference in volume fractions on both sides, $\Delta\phi = \phi_{cyt} - \phi_{ER}$. Taking into account the concentration ranges for cytoplasm and ER given by the inequalities (8) and (9), $\Delta\phi$ may take values from -0.12 to 0.26. Figure 3(a) shows the free energy for translocation of a chain with 560 monomers, for the extreme cases $\Delta\phi = -0.12$

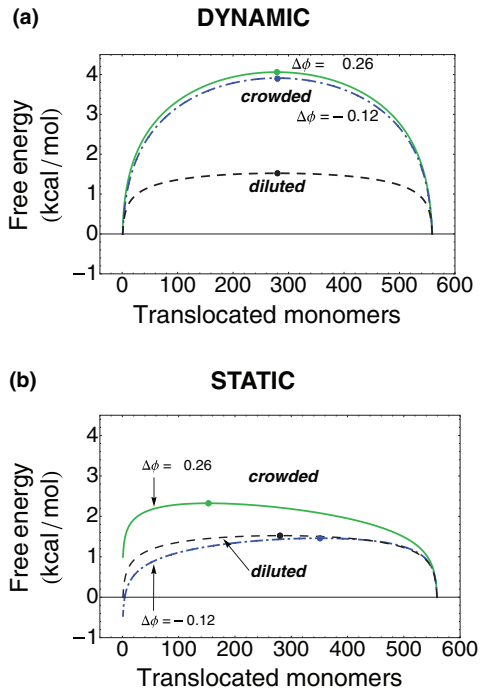

FIG. 3. (Color online) Free energy of translocation as a function of the number of translocated monomers, for a medium-sized chain like Ero1p ($N = 560$ monomers), calculated using (a) the dynamic-crowding model in Eq. (7) and (b) the static-crowding model in Eq. (10). The solid lines correspond to volume fractions $\phi_{cyt} = 0.38$ and $\phi_{ER} = 0.12$, and the dotted lines to $\phi_{cyt} = 0.12$ and $\phi_{ER} = 0.24$. These lines demarcate all free-energy curves obtained as the volume fractions in the cytoplasm and ER vary over their physiological ranges. For comparison, the dashed line shows the free energy of translocation for the diluted regime. The dots indicate the location of the maximum of each curve.

and $\Delta\phi = 0.26$. All other cases were in the narrow region bounded by these extremes. Figure 3(a) also shows that the barriers in the dynamic-crowding regime were noticeably higher than for the diluted case. The barriers were only slightly asymmetric, which cannot be seen in the scale of the graph: The two minima of the free energy for the chain fully at the cytoplasm or ER side differ just by a few tenths of kcal/mol and the maximum corresponded to translocation of almost half of the chain. As an instance, for $\Delta\phi = 0.26$ the activation energy for translocation $E_a = 3.89$ kcal/mol was only slightly smaller than the value $E_a = 4.06$ kcal/mol for retrotranslocation. Therefore, the main effect of dynamic crowding on the free energy is a substantial increase in the activation energy for translocation and retrotranslocation as compared with the diluted case.

By contrast, Fig. 3(b) shows the results for the free energy of translocation in the static-crowding regime, again for $N = 560$, for the extreme values of the volume fraction difference $\Delta\phi$ between cytoplasm and ER sides. Contrary to the case of dynamic crowding, we found that the free energy of translocation could become very asymmetric. First, the difference in free energy for chains fully in the cytoplasm and the ER lumen went from -0.46 to 1.00 kcal/mol as we increased $\Delta\phi$ through its physiological range. Secondly, the maximum shifted from $n = N/2$ in the direction of the more crowded side: by 25% towards ER when $\Delta\phi = -0.12$, and by -45%, towards cytoplasm, when $\Delta\phi = 0.26$. Compared with the dynamic-crowding case, these changes were more noticeable and sensitive to the difference in crowding agent concentration. Such sensitivity manifested as the larger area between the free energy curves for the extreme values of $\Delta\phi$.

The asymmetry in the free energy by static crowding resulted in a wider range of activation energies as we varied $\Delta\phi$: for instance, by increasing $\Delta\phi$, the activation energy of translocation decreased from 1.9 to 1.3 kcal/mol, while that of retrotranslocation increased from 1.4 to 2.3 kcal/mol. This means that, at the largest value of $\Delta\phi$, the activation energy of retrotranslocation is bigger than that of translocation by 1 kcal/mol. In contrast to the dynamic case, these ranges included the activation energy of the diluted system (1.52 kcal/mol).

What happens to the activation energy as one varies the chain size? Figure 4 shows the increase in the activation energy for translocation and retrotranslocation as the chain size was increased, for the diluted, dynamic-crowding, and static-crowding systems. Again, we illustrated the effect of changing the difference in volume fractions ($\Delta\phi$) between cytoplasm and ER with shaded regions.

For the dynamic-crowding system, changing $\Delta\phi$ has a minimal impact on the activation energies and, therefore, the shaded regions were rather thin, both for translocation and retrotranslocation situations [see Figs. 4(a) and 4(c)]. From this behavior and the form of Eq. (7) for the dynamic-crowding free energy, we deduced that the main contribution to translocation free energy comes from the confinement entropy penalty, which is independent of the volume fractions.

The rapid increase of the activation energy with chain size was more significant for dynamic-crowding systems; it was much faster than the corresponding one in the diluted case that grew as $\approx \frac{1}{2} k_B T \ln(N/4)$. We illustrated this effect by highlighting in Fig. 4 the activation energies for $N = 70$, 157, 560, and 4536, which correspond to the number of monomers in the proteins prepromelittin, ERp18, Ero1p, and ApoB. By going from diluted conditions to dynamic-crowding ones, the activation energies for these chains grew by a factor of 1.7, 2.0, 2.6, and 4.0, respectively. We noticed also that the activation energies for these chains were between 1 and 10 kcal/mol; hence, they were noticeably larger than the thermal energy at physiological conditions, $k_B T = 0.62$ kcal/mol. For a detailed comparison, we provide specific values in Table III. In cells, the energy used to overcome the activation energy may be obtained from ATP hydrolysis; under cellular conditions, the energy liberated by this process is $\Delta G_{ATP} = 14.3$ kcal/mol [70], which was of the same order of magnitude as the activation energies obtained above, especially for the larger chains.

Figures 4(b) and 4(d) show the activation energies of translocation and retrotranslocation, as functions of chain size, for the static-crowding systems. They stayed close to the results for the diluted system, for chains of all sizes considered. The effect of varying the volume fraction difference $\Delta\phi$ was almost independent of chain size, although it is larger than for the dynamic system as indicated by the wider shaded regions. In the case of static crowding, we found that it

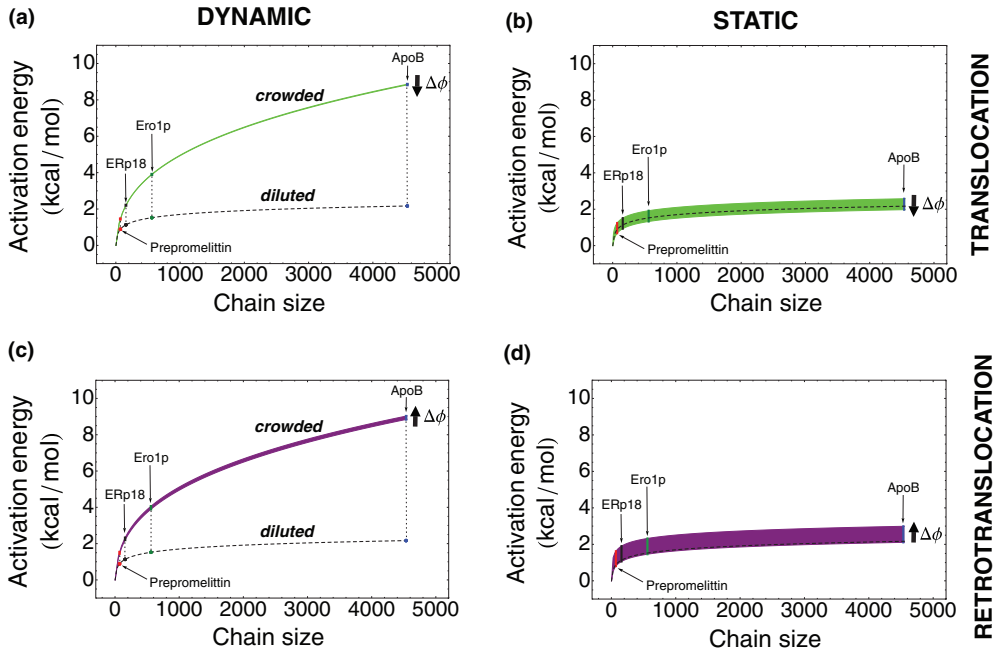

FIG. 4. (Color online) Activation energy for transport of chains across the ER membrane for different directions and regimes: (a) dynamic-crowding translocation, (b) static-crowding translocation, (c) dynamic-crowding retrotranslocation, and (d) static-crowding retrotranslocation. Shaded regions represent all values of the activation energy obtained as the volume fractions in the cytoplasm and ER vary over their physiological ranges; the dashed lines correspond to the activation energy in the diluted regime. The black thick arrows indicate the increase in the volume fraction difference $\Delta\phi = \phi_{\rm cyt} - \phi_{\rm ER}$, and the thin arrows highlight activation energies corresponding to proteins prepromelittin, ERp18, Ero1p, and ApoB.

was possible to change the relative value of the translocation and retrotranslocation activation energies by tuning the value of $\Delta\phi$. For instance, for the chains prepromelittin, ERp18, Ero1p, and ApoB, the largest increment in the activation energies of translocation as compared with the diluted case, were by a factor of 1.3, 1.4, 1.3, and 1.2, respectively. In retrotranslocation, for the mentioned chains, the largest increment in the activation energies were 1.8, 1.7, 1.5, and 1.4, respectively. By contrast, the activation energy could be reduced at most by a factor between 0.8 and 0.9 for all chains in translocation, and between 0.9 and 1 in retrotranslocation (see values in Table IV). Therefore, for static systems, one could expect to adjust the relative size of the translocation and retrotranslocation times by tuning the activation energies through $\Delta\phi$. We come back to this point later on in the section about translocation times after we discuss the forces associated with the free energy of translocation.

TABLE III. Activation energies E_a (in kcal/mol) for several values of chain size N, under diluted and dynamic-crowding conditions. Columns labeled Trans give values for transport from cytoplasm to ER lumen and those labeled Retro for transport in the opposite direction. In the diluted system, there is no difference due to direction of transport.

			Crowded[a]			
			$\Delta\phi = -0.12$		$\Delta\phi = 0.26$	
Analog	N	Diluted	Trans	Retro	Trans	Retro
Prepromelittin	70	0.9	1.5	1.4	1.4	1.5
ERp18	157	1.1	2.2	2.2	2.2	2.3
Ero1p	560	1.5	3.9	3.9	3.9	4.1
–	1000	1.7	5.0	4.9	4.9	5.1
ApoB	4536	2.2	8.9	8.8	8.8	9.0

[a]For the crowded case with $\Delta\phi = -0.12$ we set $\phi_{\rm cyt} = 0.12$ and $\phi_{\rm ER} = 0.24$, while for $\Delta\phi = 0.26$ we used $\phi_{\rm cyt} = 0.38$ and $\phi_{\rm ER} = 0.12$.

TABLE IV. Activation energies E_a (in kcal/mol) for several values of chain size N, under diluted and static-crowding conditions. Columns labeled Trans give values for transport from cytoplasm to ER lumen and those labeled Retro for transport in the opposite direction. In the diluted system, there is no difference due to direction of transport.

			Crowded[a]			
			$\Delta\phi = -0.12$		$\Delta\phi = 0.26$	
Analog	N	Diluted	Trans	Retro	Trans	Retro
Prepromelittin	70	0.9	1.2	0.8	0.7	1.6
ERp18	157	1.1	1.5	1.1	0.9	1.9
Ero1p	560	1.5	1.9	1.4	1.3	2.3
–	1000	1.7	2.1	1.6	1.5	2.5
ApoB	4536	2.2	2.6	2.1	2.0	3.0

[a]For the crowded case with $\Delta\phi = -0.12$ we set $\phi_{\rm cyt} = 0.12$ and $\phi_{\rm ER} = 0.24$, while for $\Delta\phi = 0.26$ we used $\phi_{\rm cyt} = 0.38$ and $\phi_{\rm ER} = 0.12$.

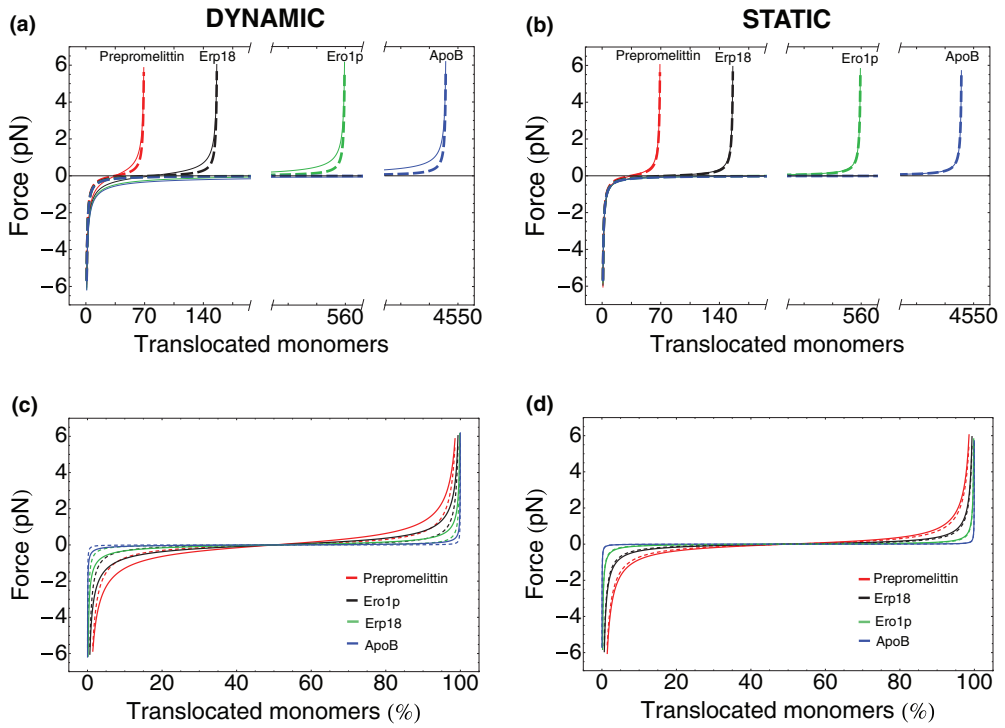

FIG. 5. (Color online) Translocation force of chains of different sizes, as a function of the number of translocated monomers for (a) dynamic-crowding conditions and (b) static-crowding conditions; and as a function of the percentage of translocated monomers for (c) dynamic-crowding conditions and (d) static-crowding conditions. Chain sizes of $N = 70$, 157, 560, and 4536, correspond, respectively, to the number of monomers in proteins prepromelittin, ERp18, Ero1p, and ApoB. In each graph, solid lines show results for the crowded conditions with $\phi_{\rm cyt} = \phi_{\rm ER} = 0.24$ and can be compared with the dashed lines corresponding to results for the diluted system ($\phi_{\rm cyt} = \phi_{\rm ER} = 0$).

C. Translocation force is intense mainly at the beginning and end of transport

Experimentally, translocation force may be more amenable to measurement than free energies or activation energies. From the free energy models, the force can be computed as the derivative of free energy with respect to the contour length of the chain that has been translocated, $L = b\,n$; that is,

$$f\,(n) = -\frac{d\mathcal{F}}{dL} = -\frac{1}{b}\frac{d\mathcal{F}}{dn}. \qquad (18)$$

Using this equation, Fig. 5 compares the translocation forces for chains of different lengths, for the cases of dynamic and static crowding with the diluted case; results for retrotranslocation forces were similar.

In all three cases, the magnitude of the force was at its maximum at the beginning and end of translocation: In the beginning, the force opposes translocation, but then its magnitude decreases rapidly. The force then changes sign and starts favoring translocation, rising rapidly again at the end of translocation. The initial force was practically independent of the chain size. In addition, it was similar for the diluted, static- and dynamic-crowding systems: For prepromelittin $N = 70$, the maximum force was 5.56 pN in the diluted system, 5.87 pN in the dynamic system, and 6.04 pN in the static system (the latter two at $\phi_{\rm cyt} = \phi_{\rm ER} = 0.24$). For the larger chain ApoB $N = 4536$, the corresponding values were 5.64 pN, 6.19 pN, and 5.71 pN.

In the three regimes, only a few monomers had to be translocated at the beginning in order to reduce the force opposing translocation considerably. The main difference among the cases was that the number of monomers needed to reduce the strength of the force was larger for the dynamic-crowding system than for the diluted or the static systems: In Fig. 5(a) the curves for the dynamic-crowding case separate noticeably from those of the diluted case. By contrast, in Fig. 5(b), the curves for the static-crowding system are almost superimposed to the diluted-case one, although the initial force decreased slightly with chain size, in contrast to the dynamic case. Likewise, the force favoring the end of translocation was intense only when a few monomers were left to translocate. The actual number increased slowly with chain size; it was also bigger for dynamic crowding than for the diluted system.

To highlight the importance of the force during the translocation process, in Figs. 5(c) and 5(d) the force is shown as a function of the percentage of translocated monomers for different chains. For the three regimes, the persistence of the force is larger for the dynamic case than either for the diluted or static-crowding systems, and the effect is more noticeable for small chains. For instance, in order to reduce the translocation force to less than 0.1 pN one needs to translocate 36% of monomers of prepromelittin and 1.2% of ApoB. These numbers increased to 43% and 8%, respectively, under dynamic-crowding conditions.

We compared our results with different estimations of the forces provided by SecA and Hsp70 proteins, proteins that assist translocation in bacteria and eukaryotes, respectively. By using the expression of Marden and Allen, which relates the force delivered by a molecular motor to its mass raised to

TABLE V. Comparison of translocation and retrotranslocation times τ under diluted and dynamic-crowding conditions, for chains with different size N and volume-fraction difference $\Delta\phi = \phi_{cyt} - \phi_{ER}$. The large increase of these times with chain size is indicated by using different units for each row.

			Crowded			
			$\Delta\phi = 0.00$		$\Delta\phi = 0.14$	
Analog	N	Diluted	Trans	Retro	Trans	Retro
Prepromelittin	70	3.0 μs	17 μs	16 μs	32 μs	36 μs
ERp18	157	21 μs	238 μs	228 μs	436 μs	476 μs
Ero1p	560	0.4 ms	30 ms	30 ms	50 ms	58 ms
	1000	1.7 ms	430 ms	426 ms	682 ms	824 ms
ApoB	4536	58 ms	56 min	56 min	80 min	103 min

the power 2/3 [71], we computed the following forces: 2.7 pN for monomeric SecA and 2.2 pN for BiP (an Hsp70 protein). As a second estimation, Alder and Theg indicated 11 pN for SecA and 28 pN for Hsp70 chaperons. They assumed that the energy from the ATP hydrolysis is converted completely into mechanical work to drive translocation [70]. A similar result for the force of the lumenal chaperon mtHsp70 in the mitochondrial matrix, between 10 and 20 pN, was obtained by De Los Rios *et al*. [72]. All of these estimated forces were in the range of 2–28 pN, with those of Alder and Theg being the biggest. By comparison with the results for the diluted and crowded systems, the maximal force of approximately 6 pN (at the beginning or the end) was of the same order of magnitude, and represented about 20% of the value estimated by Alder and Theg for Hsp70 and about 50% the value for SecA. Therefore, we conclude that the entropic forces associated with excluded volume interactions contribute significantly to translocation and retrotranslocation forces, especially at the beginning and the end of transport through the membrane.

D. Translocation time is increased markedly in the dynamic-crowding regime

We calculated the mean first-passage time for diluted and crowded systems by numerical integration of Eq. (2), using the MATHEMATICA software, version 8.0 [73]. Tables V and VI give the values obtained for different chain sizes, under several concentration conditions for diluted and crowded systems.

For the diluted system, we fitted the translocation times with a power law in chain size, and we obtained $\tau = \tau_0 N^m$, with $\tau_0 = (155.0 \pm 0.1)$ ps and $m = 2.3450 \pm 0.0001$. This result was similar to the power law $\tau \sim N^{2+p}$ of Sung and Park [26], where the value $p = 1/3$ was related to the law for the diffusion coefficient, $D \sim N^{-p}$, for protein chains in water. For the chain sizes considered, the translocation time varied from 3.0 μs for $N = 70$ (prepromelittin) to 58 ms for $N = 4536$ (ApoB). For the crowded systems, the translocation and retrotranslocation times do not need to be equal, depending on the degree of crowding on both sides of the membrane. Figure 6 illustrates this, showing the translocation and retrotranslocation times corresponding to all possible values of the volume-fraction difference $\Delta\phi$ for the fixed value $N = 560$.

Under dynamic-crowding conditions, the range of possible translocation times went from 30 to 50 ms while for retrotranslocation τ was between 30 and 58 ms. These values were significantly higher than the corresponding value of 0.4 ms in the diluted case, shown as a dot in Figs. 6(a) and 6(c). The dynamic translocation and retrotranslocation times were similar at low-crowding conditions, but at high crowding the difference between them increased with chain size. This can be observed in Fig. 6 for Ero1p and for other chains from Table V.

Unexpectedly, with dynamic crowding, the translocation and retrotranslocation times increased when the volume fractions in either the cytoplasm or ER lumen were increased while keeping the other constant; this is shown in Fig. 6. Such an outcome was due to a combination of the effects of crowding in the free energy and the diffusion coefficient. By dynamic crowding, an increment in the concentration at either side of the membrane leaves the free energy approximately the same but lowers the diffusion coefficient; that reduction resulted in a longer translocation time. As another result of dynamic crowding, in Figs. 6(a) and 6(c) it can be seen that the retrotranslocation time grew faster with changes in the cytoplasm concentration ϕ_{cyt} than the translocation time did.

For static-crowding conditions, the ranges of the transport times for $N = 560$ were much closer to the diluted case than in the dynamic-crowding case: In translocation, they went

TABLE VI. Comparison of translocation and retrotranslocation times τ under diluted and static-crowding conditions, for chains with different size N and volume-fraction difference $\Delta\phi = \phi_{cyt} - \phi_{ER}$. The large increase of these times with chain size is indicated by using different units for each row.

			Crowded[a]			
			$\Delta\phi = -0.12$		$\Delta\phi = 0.26$	
Analog	N	Diluted	Trans	Retro	Trans	Retro
Prepromelittin	70	3.0 μs	19 μs	10 μs	13 μs	45 μs
ERp18	157	21 μs	203 μs	100 μs	124 μs	383 μs
Ero1p	560	0.4 ms	8.7 ms	3.7 ms	4.3 ms	11 ms
–	1000	1.7 ms	48 ms	20 ms	22 ms	53 ms
ApoB	4536	58 ms	4.3 s	1.6 s	1.8 s	3.4 s

[a]Under static crowded conditions, the minimum and maximum times were obtained at ($\phi_{cyt} = 0.12, \phi_{ER} = 0.24$) and ($\phi_{cyt} = 0.38, \phi_{ER} = 0.12$), for translocation or retrotranslocation.

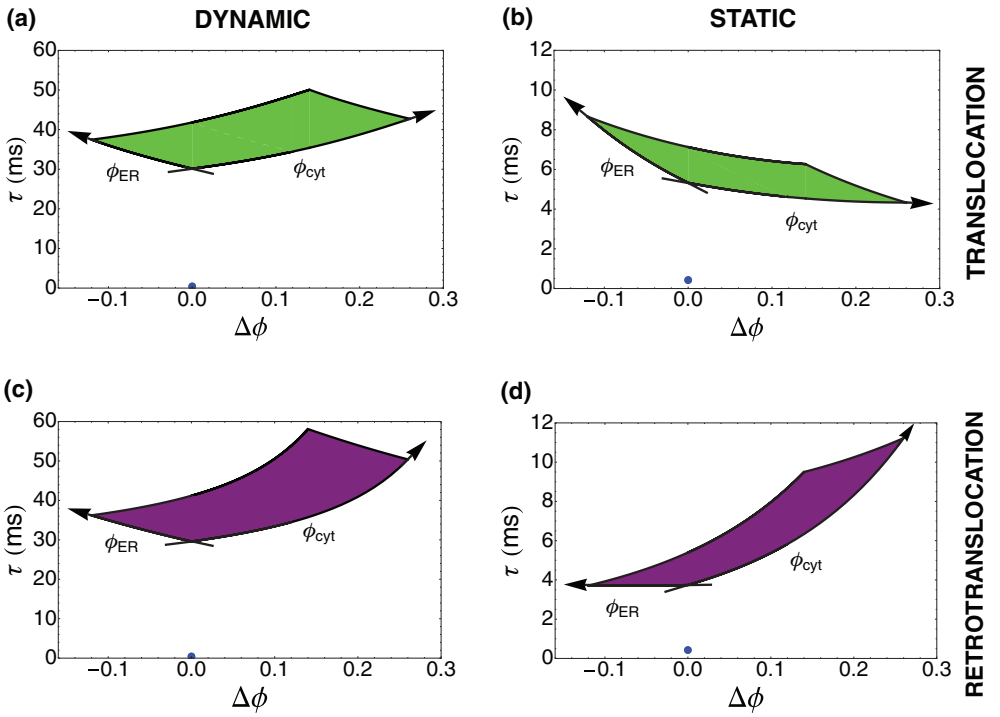

FIG. 6. (Color online) Transport time τ for Ero1p ($N = 560$ monomers) as a function of volume fraction difference $\Delta\phi = \phi_{cyt} - \phi_{ER}$ for (a) dynamic-crowding translocation, (b) static-crowding translocation, (c) dynamic-crowding retrotranslocation, and (d) static-crowding retrotranslocation. The shaded regions indicate the values of τ obtained for every combination of volume fractions in the physiological ranges $0.12 \leqslant \phi_{ER} \leqslant 0.24$ and $0.12 \leqslant \phi_{cyt} \leqslant 0.38$. Arrows indicate the effect of increasing ϕ_{ER} or ϕ_{cyt} while keeping the other volume fraction fixed. For comparison, the blue dots near the origin in each graph indicate the transport time for the diluted system ($\phi_{cyt} = \phi_{ER} = 0$).

from 4.3 to 8.7 ms; for retrotranslocation they covered a larger interval, from 3.7 to 11.0 ms [see Figs. 6(b) and 6(d)]. On the other hand, contrary to the dynamic case, the static translocation and retrotranslocation times could be rather different. For instance, when the ER is most concentrated with respect to the cytoplasm ($\Delta\phi = -0.12$) the static translocation time was twice the retrotranslocation time. At the other extreme, when the cytoplasm is most concentrated with respect to the ER ($\Delta\phi = 0.26$), the static translocation time was only one-third of the retrotranslocation time (see data of Table VI).

With static crowding, it was possible to reduce the translocation time τ by increasing the concentration in the cytoplasm [see Fig. 6(b)] because the change in the free energy overcomes the reduction in the diffusivity. The other way to reduce the translocation time was by decreasing the ER concentration, which again introduced a favorable change in the free energy but now increasing the diffusivity in the ER. Similar results to reduce the transport time also applied to the retrotranslocation process as depicted in Fig. 6(d). This way to reduce the transport time by static crowding is opposite to the dynamic-crowding case where the diffusion coefficient dominated the transport.

Varying the chain size has a great impact on the translocation times; Fig. 7 illustrates this by plotting the range of all times for transport across the membrane corresponding to the physiological ranges of ϕ_{cyt} and ϕ_{ER}. Focusing first on the dynamic-crowding systems, we observed that translocation and retrotranslocation times increased steeply with N: For chains with several thousand monomers both times were on the order of minutes and even more than an hour [see Figs. 7(a) and 7(c)]. The corresponding times in the diluted case, growing as $N^{7/3}$, appeared practically constant in the same scale. In addition, for a given chain, we observed that the dynamic retrotranslocation time could become larger than the dynamic translocation time, and had a wider range as ϕ_{cyt} and ϕ_{ER} were varied.

For a more detailed comparison, Table V gives translocation times, of chains with different sizes, for the diluted system and for two dynamic-crowding cases that delimit the minimum and maximum translocation times: $\tau(\phi_{cyt} = 0.12, \phi_{ER} = 0.12)$ and $\tau(\phi_{cyt} = 0.38, \phi_{ER} = 0.24)$. The ratio of the dynamic- to the diluted-regime translocation times for chains of different lengths gives a quantitative indication of the importance of the effect of dynamic-crowding conditions. For short chains, with a few tens of monomers, this ratio was of order 10. For medium chains, with several hundred monomers, it increased to 100. For very large chains, of several thousand monomers, the ratio became as large as 10 000. Accordingly, the dynamic translocation time went from a few microseconds for short chains, to tens of milliseconds for medium chains, to hours for large chains (for particular values, see Table V).

The transport times in the diluted system differed markedly from the ones in dynamic-crowded conditions. The calculation of the transport times was based simultaneously on the diffusivity and free energy models used. To shed light on the contribution from each one, we computed the translocation time with two additional hybrid models: The first one had the free energy model for diluted conditions

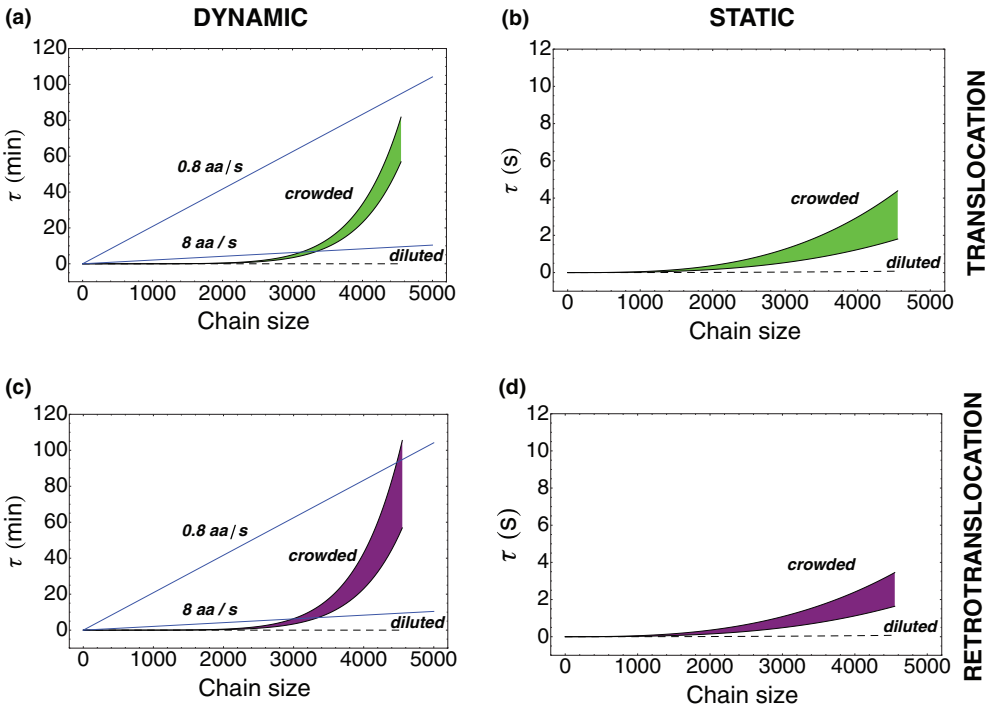

FIG. 7. (Color online) Transport time τ as a function of the chain size N for (a) dynamic-crowding translocation, (b) static-crowding translocation, (c) dynamic-crowding retrotranslocation, and (d) static-crowding retrotranslocation. Shaded regions indicate all values of τ obtained by varying the volume fractions in the cytoplasm and ER lumen within their physiological ranges. The dashed lines indicate the corresponding results in the diluted regime. The solid lines in (a) and (c) correspond to the slowest and fastest translocation rates reported in Refs. [5] and [7], respectively, for experiments performed under diluted conditions.

and the dynamic-crowding diffusivity; the second one had the dynamic-crowding free energy and the diluted-conditions diffusivity. Taking the diluted system as a reference, the first hybrid model let us quantify the change in the translocation time by changing the diffusivity model, and the second one, the change by the free energy.

In the first hybrid model, the translocation time grew by a factor between one for small chains and a few tens for large chains; in the second hybrid model the factor was close to 1 for small and medium chains but was on the order of 1000 for large chains. None of these results matched the very large ratio of 10 000 for the dynamic- to diluted-translocation time of large chains. This means that there was synergy between the diffusivity and the free energy effects as we changed the size of the chain and the crowded conditions. For the largest chain, ApoB, the time scale imposed by the change in the free energy from the diluted to the crowded system (10^3), multiplied by that corresponding to the change in diffusivity (10), gives rise to the 10 000 factor observed when both changes were present.

Now, for the static-crowding system, we observed that increasing N resulted in increased translocation and retrotranslocation times, but they never grew as much as in the dynamic-crowding system: The static translocation and retrotranslocation times were just on the order of a few seconds even for chains with thousands of monomers. This is shown in Figs. 7(b) and 7(d) along with the diluted-system time which seemed practically constant on the scale of the static-crowding times. As compared with the diluted case, static crowding with $\phi_{\mathrm{cyt}} = 0.12$ and $\phi_{\mathrm{ER}} = 0.24$ increased the translocation time by a factor of six for short chains as prepromelittin; 22 for average chains, as Ero1p, and 74 for larger chains, as ApoB. The increase by static crowding was not as stunning as that of dynamic crowding.

In eukaryotes, chaperones in the ER side bind to the translocating chain and are thought to speed up translocation by acting as ratchets that avoid backward translocation [27]. A model that includes ratchets is that of Simon *et al.* for a one-dimensional chain [74]. In their model, one or multiple ratchets can act on the translocated segment along the chain. For one chain of 100 nm ($N \approx 263$ aa) with diffusion coefficient of 1 $\mu\mathrm{m}^2/\mathrm{s}$, the Simon *et al.* model predicts 5 ms for the translocation time when there is a single ratchet acting. From our results, the predicted times for the same chain were 0.07 ms in the diluted system and 1.5–2.6 ms in the dynamic-crowding one, which were of similar magnitude to the results of Simon and co-workers.

We next compared our results with experimental data for translocation in *in vitro* systems. As indicated in the introduction, experiments with inverted membrane vesicles and proteoliposomes (in the presence of ATP and chaperones that promote translocation) have reported different values for the translocation rate, that is, the number of amino acids translocated per second. For forward translocation of proOmpA derivatives, the translocation rate was found as 0.8–1 aa/s in proteoliposomes and 2.5 aa/s in inverted membrane vesicles (IMVs) [5]. The translocation rate for in-tandem constructs of proOmpA, whose length range from

347 to ∼1400 amino acids, was 4.5 aa/s in IMVs [6]. From the translocation times in IMVs, a translocation rate of 8 aa/s can be computed for proOmpAHisC constructs that range from 200 to ∼550 amino acids [7]. Therefore, we may consider the transport rates in diluted conditions to be between 0.8–8 aa/s. From our results, we computed the average transport rates as $v = N/\tau$.

For diluted conditions, the translocation rates for the representative chains prepromelittin, Ero1p and ApoB were found to be, respectively, 2.4×10^7, 1.4×10^6, and 7.8×10^4 aa/s. For static conditions with $\phi_{\mathrm{cyt}} = 0.38$ and $\phi_{\mathrm{ER}} = 0.12$, the respective values were 5.4×10^6, 1.3×10^5, and 2.5×10^3 aa/s. Finally, for dynamic conditions with $\phi_{\mathrm{cyt}} = 0.12$ and $\phi_{\mathrm{ER}} = 0.12$, the corresponding rates were 4.1×10^7, 1.9×10^4, and 1.4 aa/s. The concentrations given above for the static and dynamic conditions yield the maximum translocation rates; results for other crowding conditions within the physiological range were of the same order of magnitude.

From this comparison, we can see that the theoretical translocation rates for diluted conditions (from our model or that of Simon *et al*. [74]) do not coincide with the rates from experiments in diluted systems. In spite of a careful literature review, we are not aware of any measurement of posttranslational translocation rates in crowded systems, neither *in vivo* nor *in vitro*, to compare with our results for the two crowded cases. Therefore, we can only compare the crowding calculations with the experimental data for diluted conditions. The static translocation rates were several orders of magnitude larger than the diluted ones, for all chains considered. The dynamic translocation rates for small and average size chains were also larger than the diluted ones, but for large chains with thousands of monomers the rates were within the experimental range for the diluted systems (see Fig. 7).

The large discrepancy in the translocation rates, primarily under diluted conditions, makes us conclude that additional interactions, besides the steric ones, need to be incorporated into the model. Such interactions, independently of the origin, should be quite strong to lower the translocation rates by several orders of magnitude.

On the other hand, in the absence of experimental data of translocation in systems crowded by proteins at physiological concentrations, as happens in translocation *in vivo*, our results indicated a marked difference between translocation in diluted and crowded systems. This difference grows with the degree of crowding, increases with the size of the chain, and becomes more marked with dynamic crowding conditions that correspond with biological milieus where proteins are translocated.

IV. CONCLUSIONS

We have studied the physical properties of protein translocation in the two different crowded regimes described by Gopinathan and Kim [25]. We stress that this model implicitly assumes normal diffusion since it is based on the Fokker-Planck equation, which does not account for subdiffusion of the kind reported in recent experiments [22–24].

These regimes, which take into account the steric interaction of crowding, were the static and the dynamic regime, where spherical crowding agents seem to be immobile or diffusing fast, respectively, as compared with the movement of the translocating chain. We have highlighted the dynamic regime, which resembles biological environments where proteins are translocated. The crowding conditions used were those found in the cytoplasm of eukaryotic and bacterial cells and the lumen of the ER. We quantified the effect of crowding by comparing the translocation free energy, activation energy, force, and transport times, with those of a chain translocating in a diluted system.

We found that dynamic crowding increased the free energy and, as a consequence, also the activation energy. Bigger chains caused much higher activation energies: There was a twofold increase for the smallest protein, prepromelittin, and up to a fourfold increment for the largest, ApoB, as compared with that in diluted conditions. The force, from an entropic origin, was important for the first and the last translocated monomers: at the beginning being opposite to translocation, at the end, pushing in favor of translocation. Crowding slowed down the decay rate of the force compared with the dilute case, which means that more work is needed to carry out translocation.

We included the dynamical behavior of proteins, in diluted and crowded milieus for the computation of the transport times, by using fits to experimental diffusion coefficients. In the diluted system, the translocation times were proportional to a power law for the size of the chain N. The exponent $2 + p$ in this law agreed with the results of Sung and Park, with p being the exponent in the model for the diffusion of polymers. When dynamic crowding was included, there was a delay in the transport times for the crowded conditions tested. An increase in the volume fraction in one side of the membrane, while keeping the other fixed, increased the dynamic translocation and retrotranslocation times by a factor depending on the size of the chain: few-fold times for small chains and up to 10 000 times for large chains. We showed that such a huge increase comes from the synergy between the free energy and the diffusion of the translocating chain, which indicates that neither contribution can be overlooked when studying translocation. The translocation rates (in amino acids per second) for large chains in the dynamic-crowding system were similar to those from experiments in diluted conditions, which means that the effect of crowding may be measured experimentally. This result is important from the biological standpoint because it tells how the posttranslational translocation process behaves at physiological crowded conditions.

With static crowding, only slight modifications of the physical properties of translocation and retrotranslocation were detected: the free energy, the activation energy, and the forces were similar to those of the diluted case. The translocation and retrotranslocation times grew but not at the same level that dynamic crowding does. Static crowding increased the transport times a few fold for small chains and a few tenfold for large chains, as compared with the diluted case. Although the static regime considered here does not correspond to the biological milieus for protein translocation between cytoplasm and ER lumen, it illustrates how macromolecular crowding by static agents can modify the transport properties of translocation.

In summary, our results indicate a clear difference between the translocation in a diluted system and a system crowded at physiological conditions. Interestingly, such a crowded

environment must be of the dynamic type in order to resemble biological milieus; that condition is precisely responsible for the huge change for all physical properties of translocation. Surprisingly, the lack of movement in the static regime leads to similar properties of translocation as the diluted case. The results for the dynamic-crowding regime, which correspond to biological systems, indicate that effects of crowding cannot be neglected when studying translocation because the steric contribution of crowding changes the properties of translocation.

ACKNOWLEDGMENTS

J.A.V.P. and O.G.L. acknowledge support from Red de Materia Condensada Blanda (Conacyt, Mexico) and UC-MEXUS-Conacyt (Project No. CN-10-396). The authors also thank Professor Roland Faller and Professor Michel Picquart for insightful discussions.

APPENDIX: FITS OF PROTEIN DIFFUSIVITIES IN THE CYTOPLASM AND ER LUMEN

We fitted the data for protein diffusivities in the cytoplasm, across all cell types, with the expression

$$D(N) = AN^{-p}, \tag{A1}$$

and obtained $p = 0.59 \pm 0.11$ and $A = 344 \pm 226$ μm^2/s. Figure 2(a) shows this fit as a dashed line. Fitting separately for each cell type, we found values of p in the range 0.40–0.76: for instance, for soleus muscle cells at 22 °C, $p = 0.55 \pm 0.04$. These values for p are close to the Zimm limit, so we repeated the collective fit setting $p = 1/2$, obtaining $A = 197 \pm 21$ μm^2/s. In Fig. 2, this simpler fit is shown as a solid line, which is also very good, so we adopted it for the rest of the work.

Now, for the dependence with the volume fraction ϕ, there are several experimental works with artificial systems built to mimic physiological crowding concentrations [51,52] which indicate an exponential dependence of the diffusivity with ϕ, i.e., $\log D \sim -\phi$. More recently, Konopka *et al.* measured the diffusivity of green fluorescent protein (GFP) in the cytoplasm of *Escherichia coli* [54]. They changed the protein concentration in the cytoplasm by growing cells under different values of osmolality (between 0.28 and 1.45 osm). Their data for cells adapted to such osmolality conditions also follow an exponential dependency with ϕ, as shown in Fig. 2.

We fitted the GFP data by Konopka and co-workers with the expression

$$D(\phi) = B\exp(-\gamma\phi). \tag{A2}$$

The parameters found were $B = 28 \pm 13$ and $\gamma = 4.2 \pm 1.9$. The resulting fit, as shown in Fig. 2, was also good.

We combined the exponential fit for volume fraction and the power law for chain size to obtain a combined expression of the form given by Eq. (13):

$$D_{\rm cyt}(N,\phi) = D_0 N^{-1/2} e^{-4.2\phi}. \tag{A3}$$

The constant D_0 can be found by substitution of $N = 238$ for GFP and matching the result with the fit to Konopka *et al.* data. The result was $D_0 = B\sqrt{238} = 433$ μm^2/s.

By using Eq. (A1), we fitted the data of Table II for the ER lumen diffusivity of chains with different lengths and obtained $p = 1.24 \pm 0.26$ and $A = 8477 \pm 12484$ μm^2/s. The corresponding fit is shown in Fig. 2(a) as the red-dashed line. This procedure with two adjustable parameters resulted in a very large uncertainty for A, although the fitted exponent was close to that of the Rouse model. We decided to fix the exponent of the power law to its Rouse value, $p = 1$, and fit just one parameter. The value obtained was $A = 2139 \pm 168$ μm^2/s; the corresponding fit is shown in Fig. 2(a) as the red, solid line. These two models gave very similar values for the diffusivity in the ER, but we used the second one (Rouse) exclusively for all subsequent calculations.

To establish the expression of $D(\phi)$ for the ER lumen we proceeded as follows. First, we assumed that, as in the cytoplasm, the diffusivity as a function of ϕ follows the exponential law given in Eq. (A2). Then, we used experimental values of the diffusion coefficient in cells from Dayel *et al.* [16], where the extracellular osmolalities were changed. The measured value for the diffusion coefficient of the GFP in the ER lumen of CHO-K1 cells was 7.5 ± 2.5 μm^2/s. When the extracellular osmolality was changed, a 1.3-fold reduction of the diffusion coefficient occurred in going from 0.15–0.45 osm to 0.60 osm. Assuming that an increase in the external osmolality increases the protein content, being capable of reaching its highest value at high osmolalities (amounting to $\phi_{\rm ER} = 0.24$), we found $B = 9.7 \pm 3.3$ μm^2/s and $\gamma = 2.14 \pm 0.05$.

Likewise to the analysis of the cytoplasm diffusivity, we combined $D(N)$ and $D(\phi)$ using Eq. (13) to get the final model for the ER lumen diffusivity:

$$D_{\rm ER}(N,\phi) = (2308\ \mu{\rm m}^2\,{\rm s}^{-1}) N^{-1} e^{-2.1\phi}. \tag{A4}$$

[1] D. N. Herbert, R. Bernasconi, and M. Molinari, Semin. Cell Dev. Biol. **21**, 526 (2010).
[2] K. Bagola, M. Mehnert, E. Jarosch, and T. Sommer, Biochim. Biophys. Acta **1808**, 925 (2011).
[3] F. Navarro-García, A. Canizalez-Roman, K. E. Burlingame, K. Teter, and J. E. Vidal, Infect. Immun. **75**, 2101 (2007).
[4] C. C. Chow, C. Chow, V. Raghunathan, T. J. Huppert, E. B. Kimball, and S. Cavagnero, Biochemistry **42**, 7090 (2003).
[5] K. J. Erlandson, E. Or, A. R. Osborne, and T. A. Rapoport, J. Biol. Chem. **283**, 15709 (2008).
[6] D. Tomkiewicz, N. Nouwen, R. van Leeuwen, S. Tans, and A. J. M. Driessen, J. Biol. Chem. **281**, 15709 (2006).
[7] F.-C. Liang, U. K. Bageshwar, and S. M. Musser, Mol. Biol. Cell **20**, 4256 (2009).
[8] F. A. Agarraberes and J. F. Dice, Biochim. Biophys. Acta **1513**, 1 (2001).
[9] W. Wickner and R. Schekman, Science **310**, 1452 (2005).
[10] G. L. Perez, B. Huynh, M. Slater, and S. Maloy, J. Bacteriol. **191**, 135 (2009).

[11] S. Cayley, B. A. Lewis, H. J. Guttman, and M. T. Record Jr., J. Mol. Biol. **222**, 281 (1991).
[12] J. T. Mika and B. Poolman, Curr. Opin. Biotech. **22**, 117 (2011).
[13] T. Kühn, T. O. Ihalainen, J. Hyväluoma, N. Dross, S. F. Willman, J. Langowski, M. Vihinen-Ranta, and J. Timonen, PLoS ONE **6**, e22962 (2011).
[14] A. Forer and R. D. Goldman, J. Cell Sci. **10**, 387 (1972).
[15] G. C. Brown, J. Theor. Biol. **153**, 195 (1991).
[16] M. J. Dayel, E. F. Y. Hom, and A. S. Verkman, Biophys. J. **76**, 2843 (1999).
[17] G. Koch, M. Smith, D. Macer, P. Webster, and R. Mortara, J. Cell Sci. **86**, 217 (1986).
[18] D. R. J. Macer and G. L. E. Koch, J. Cell Sci. **91**, 61 (1988).
[19] R. J. Ellis, Trends Biochem. Sci. **26**, 597 (2001).
[20] B. van der Berg, R. J. Ellis, and C. M. Dobson, EMBO J. **18**, 6927 (1999).
[21] J. A. Dix and A. S. Verkman, Annu. Rev. Biophys. **37**, 247 (2008).
[22] I. Golding and E. C. Cox, Phys. Rev. Lett. **96**, 098102 (2006).
[23] S. C. Weber, A. J. Spakowitz, and J. A. Theriot, Phys. Rev. Lett. **104**, 238102 (2010).
[24] J.-H. Jeon, V. Tejedor, S. Burov, E. Barkai, C. Selhuber-Unkel, K. Berg-Sorensen, L. Oddershede, and R. Metzler, Phys. Rev. Lett. **106**, 048103 (2011).
[25] A. Gopinathan and Y. W. Kim, Phys. Rev. Lett. **99**, 228106 (2007).
[26] W. Sung and P. J. Park, Phys. Rev. Lett. **77**, 783 (1996).
[27] E. Park and T. A. Rapoport, Annu. Rev. Biophys. **41**, 21 (2012).
[28] D. Hizlan, A. Robson, S. Whitehouse, V. A. Gold, J. Vonck, D. Mills, W. Kühlbrandt, and I. Collinson, Cell Reports **1**, 21 (2012).
[29] B. Zhang and T. F. Miller III, J. Am. Chem. Soc. **134**, 13700 (2012).
[30] H. Risken, *The Fokker-Planck Equation: Methods of Solution and Applications*, 2nd ed. (Springer, New York, 1989).
[31] N. G. van Kampen, *Stochastic Processes in Physics and Chemistry* (North Holland, Amsterdam, 1992).
[32] R. Zimmerman, M. Sagstetter, G. Schlenstedt, H. Wiech, B. Kaßeckert, and G. Müller, in *Membrane Biogenesis*, edited by J. A. F. O. den Kamp, Vol. H16 (Springer, New York, 1988), pp. 337–350.
[33] G. Suchanek, G. Kreil, and M. A. Hermodson, Proc. Natl. Acad. Sci. USA **75**, 701 (1978).
[34] M. L. Rowe, L. W. Ruddock, G. Kelly, J. M. Schmidt, R. A. Williamson, and M. J. Howard, Biochemistry **48**, 4596 (2009).
[35] H. Ito, I. Iwamoto, Y. Inaguma, T. Takizawa, K. ichi Nagata, T. Asano, and K. Kato, J. Cell. Biochem. **95**, 932 (2005).
[36] E. Gross, D. B. Kastner, C. A. Kaiser, and D. Fass, Cell **117**, 601 (2004).
[37] R. B. Freedman, A. D. Dunn, and L. W. Ruddock, Curr. Biol. **8**, R468 (1998).
[38] A. Helenius, T. Marquardt, and I. Braakman, Trends Cell Biol. **2**, 227 (1992).
[39] J. Macri and K. Adeli, J. Biol. Chem. **272**, 7328 (1997).
[40] Z. Yao, K. Tran, and R. S. McLeod, J. Lipid Res. **38**, 1937 (1997).
[41] C.-Y. Yang, F.-S. Lee, L. Chan, D. A. Sparrow, J. T. Sparrow, and J. Antonio M. Gotto, Biochem. J. **239**, 777 (1986).
[42] M. Castelnovo, R. K. Bowles, H. Reiss, and W. M. Gelbart, Eur. Phys. J. E **10**, 191 (2003).
[43] M. Doi and S. F. Edwards, *The Theory of Polymer Dynamics* (Oxford University Press, Oxford, 1986).
[44] S. B. Zimmerman and S. O. Trach, J. Mol. Biol. **222**, 599 (1991).
[45] J. Bereiter-Han, C. H. Fox, and B. Thorell, J. Cell Biol. **82**, 767 (1979).
[46] F. Lanni, A. S. Waggoner, and D. L. Taylor, J. Cell Biol. **100**, 1091 (1985).
[47] P. Grassberger and I. Procaccia, J. Chem. Phys. **77**, 6281 (1982).
[48] P. M. Richards, Phys. Rev. Lett. **56**, 1838 (1986).
[49] P. M. Richards, J. Chem. Phys. **85**, 3520 (1986).
[50] G. T. Barkema, P. Biswas, and H. van Beijeren, Phys. Rev. Lett. **87**, 170601 (2001).
[51] E. Dauty and A. S. Verkman, J. Mol. Recognit. **17**, 441 (2004).
[52] D. S. Banks and C. Fradin, Biophys. J. **89**, 2960 (2005).
[53] R. J. Phillips, Biophys. J. **79**, 3350 (2000).
[54] M. C. Konopka, K. A. Sochacki, B. P. Bratton, I. A. Shkel, M. T. Record, and J. C. Weisshaar, J. Bacteriol. **191**, 231 (2009).
[55] M. Arrio-Dupont, G. Foucault, M. Vacher, P. F. Devaux, and S. Cribier, Biophys. J. **78**, 901 (2000).
[56] S. Popov and M. M. Poo, J. Neurosci. **12**, 77 (1992).
[57] S. Papadopoulos, K. D. Jürgens, and G. Gros, Biophys. J. **79**, 2084 (2000).
[58] S. Papadopoulos, K. D. Jürgens, and G. Gros, Pflügers Arch. **430**, 519 (1995).
[59] H. Lodish, A. Berk, C. A. Kaiser, M. Krieger, M. P. Scott, A. Bretscher, H. Ploegh, and P. Matsudaira, *Molecular Cell Biology*, 6th ed. (W. H. Freeman and Company, New York, 2007).
[60] D. M. Chudakov, M. V. Matz, S. Lukyanov, and K. A. Lukyanov, Physiol. Rev. **90**, 1103 (2010).
[61] E. L. Snapp, A. Sharma, J. Lippincott-Schwartz, and R. S. Hegde, Proc. Natl. Acad. Sci. USA **103**, 6536 (2006).
[62] C. W. Lai, D. E. Aronson, and E. L. Snapp, Mol. Biol. Cell **21**, 1909 (2010).
[63] D. L. Howarth, A. M. Vacaru, O. Tsedensodnom, E. Mormone, N. Nieto, L. M. Costantini, E. L. Snapp, and K. C. Sadler, Alcohol. Clin. Exp. Res. **36**, 14 (2012).
[64] I. Lang, M. Scholz, and R. Peters, J. Cell Biol. **102**, 1183 (1986).
[65] R. Swaminathan, C. P. Hoang, and A. S. Verkman, Biophys. J. **72**, 1900 (1997).
[66] A. M. Mastro, M. A. Babich, W. D. Taylor, and A. D. Keith, Proc. Natl. Acad. Sci. USA **81**, 3414 (1984).
[67] W. S. Price, P. W. Kuchel, and B. A. Cornell, Biophys. Chem. **33**, 205 (1989).
[68] T. Kalwarczyk, N. Ziebach, A. Bielejewska, E. Zaboklicka, K. Koynov, J. Szymański, A. Wilk, A. Patkowski, J. Gapiński, H.-J. Butt *et al.*, Nano Lett. **11**, 2157 (2011).
[69] B. R. Daniels, B. C. Masi, and D. Wirtz, Biophys. J. **90**, 4712 (2006).
[70] N. N. Alder and S. M. Theg, Trends Biochem. Sci. **28**, 442 (2003).
[71] J. H. Marden and L. R. Allen, Proc. Natl. Acad. Sci. USA **99**, 4161 (2002).
[72] P. D. L. Rios, A. Ben-Zvi, O. Slutsky, A. Azem, and P. Goloubinoff, Proc. Natl. Acad. Sci. USA **103**, 6166 (2006).
[73] Computer program MATHEMATICA, Version 8.0, Wolfram Research, Inc., Champaign, IL, 2010.
[74] S. M. Simon, C. S. Peskin, and G. F. Oster, Proc. Natl. Acad. Sci. USA **89**, 3770 (1992).